# Enhancement of Wind Turbine Performance Using Air-Blowing Technique by Modified Strong Implicit Procedure (MSIP) Optimization Solver Method

**Dr. Yasser Ahmed Mahmood**
Electromechanical Engineering Department, University of Technology/ Baghdad
**Dr. Mustafa Sami Abdullateef**
Electromechanical Engineering Department, University of Technology/ Baghdad
**Dr. Muhannad Zedan Khelifa**
Electromechanical Engineering Department, University of Technology/ Baghdad
Email: uot_techmagaz@yahoo.com
**Abdulhadi Mohammed Jawad**
South oil Company, Ministry of oil/Basrah

**Received on: 9/5/2013 & Accepted on: 4/7/2013**

**ABSTRACT:**

A powerful intensifier of friction in air flows affects the lift and drag coefficients, the flow separation plays a vital part in aerodynamic characteristics for technical applications. The porous air blowing is also one of a powerful technique that determines and improves of these characteristics. In present work the influence of this technique on power coefficient in separated laminar flow over wind turbine blade is investigated in numerical and optimization methods. The influence of some parameters associated with using air blowing, such as the speed air blowing ratio ($U_j/U$) strength on the performance of the NACA 4415 two dimensional airfoil at different angle of attack($5^o$ ،$10^o$ ،$15^o$) have been studied. The result shows that the air blowing is effective in controlling the separation in all cases but the power coefficient is greater in $\alpha = 5$ than the other angles and at tip speed ratio equal 2.5. The influence of air blowing technique on the power coefficient is clear and greater than without blowing cases.

**Keywords**:Power Coefficient, Angle of Attack, Air Blowing, Aerodynamic Characteristics, Airfoil, Separation. Tip Speed Ratio.

## تحسين أداء التوربين الهوائي بأستخدام تقنية نفخ الهواء بطريقة الحل بالأسلوب الضمني القوية المثلى (MSIP)

**الخلاصة:**

يعتبر الأحتكاك من أشد العوامل المؤثرة على معامل الرفع والكبح للهواء المنساب حيث يلعب أنفصال الهواء المنساب نتيجة الأحتكاك دوراً مهما في تحديد المواصفات الأيروديناميكية في التطبيقات التقنية. ان النفخ المسامي للهواء يعتبر أحدى التقنيات الفعالة لأيجاد وتحسين هذه المواصفات. في هذا البحث تم دراسة تأثير هذه التقنية على معامل القدرة للهواء الطباقي المنفصل على ريش التوربين

الهوائي بأستخدام طرق عددية وتحسينية مثلى، حيث تمت دراسة تأثير بعض العوامل الخاصة بأستخدام نفخ الهواء مثل شدة نسبة النفخ الى سرعة الهواء$(U_j/U)$على أداء المطيار NACA 4415 الثنائي البعد لمختلف زوايا الهجوم($5^o$، $10^o$، $15^o$). بينت النتائج ان نفخ الهواء له سيطرة فعالة على انفصال الهواء في كل الحالات ولكن معامل القدرة له قيمة أعلى ما يمكن في زاوية هجوم $\alpha = 5^o$ ونسبة السرعة النسبية 2.5 قياساً بالزوايا والنسب الاخرى. ومن الواضح، وحسب النتائج التي تم الحصول عليها في هذا البحث، تأثير تقنية نفخ الهواء على معامل القدرة كبير مقارنةً مع حالة عدم استخدام هذه التقنية.

**List of Symbols:**

$C_p$: Pressure coefficient.
c: Chord length (m).
$U_j$: Jet plowing velocity.
U, V: Mean velocity componants (m/sec.).
P: Pressure ($N/m^2$).
k : Turbulant kinetic energy ($m^2/sec^2$).
ε : Dissipation of turbulant kinetic energy ($m^2/sec^2$).

**INTRODUCTION:**

Wind turbine growth in size and weight made it impossible to control turbines passively as they were controlled in the past. Current efforts focus on increasing their aerodynamic efficiency and operational range through active flow control methods. One of the main methods of active flow control is the usage of blowing devices with constant or pulsed jets.

As stated by Bobonea A.[1], the addition of stored high-momentum air through slots into the boundary layer, they overcome adverse pressure gradients and postpone separation. Pulsed blowing sends short pulses rather than a continuous jet of fluid into the boundary layer and has been found to be more effective. Through CFD simulations over a 2D wind turbine airfoil, this research highlights the impact of different slot geometries with constant/pulsed blowing, on the effectiveness of this active flow control technique.

BokserV. D., et al[2], presented the experimental study of tangential jet blowing efficiency for improvement of supercritical wing aerodynamics at transonic speeds. The study of the wing-fuselage model were performed in the TsAGI T-106 transonic wind tunnel in Mach number ranges of $M = 0.4$ to 0.8, Reynolds number ranges of $Re = (1.4 \text{ to } 2.2)10^6$, and anglesof attack$\alpha = -2°$ to 15°. The effects of jet blowing intensity on lift, pitching moment, drag of the model and also on the pressure distribution at the wing middle section are examined.

Campbell G. A, et al [3], dealing with the aerodynamic aspect of the blown film process. An air flow field similar to that in the blown film process was produced by blowing air past a rigid model. Aerodynamic experiments were carried out to determine the velocity and pressure distributions, and the overall axial force on the rigid model. Theoretical predictions using the techniques of superposition of stream functions and macro-balances of mass and energy were compared with experimental data.

Jiang, P, et al [4], take up the effects of unsteady trailing-edge blowing on delta wing aerodynamics were investigated experimentally to understand the

aerodynamics-propulsion interaction for dynamic thrust vectoring. Two models with sweep angles of $\Lambda = 50^0 \; and \; 65^o$, representing nonslender and slender delta wings, respectively, were tested in a wind tunnel. Flow visualization and velocity and force measurements were conducted at stall and poststall incidences. For the periodic blowing, it was found that the dynamic response of leading-edge vortex breakdown and wing normal force coefficient exhibit phase lags for both nonslender and slender delta wings.

Yasser A. M. [5], to touch on the systematical investigation of the jet blowing is conducted on the NACA 2412 airfoil in the range of angle of attack from 0º to 30º included up and beyond the stall angle at a range of $Re = 9.7 \times 10^6 - 1.7 \times 10^6$ . The influence of some parameters associated with using jet blowing, such as its location, and the speed ratio $(U_j/U)$ strength on the performance of the NACA 2412 airfoil has also been studied. The result shows that the jet blowing is effective in controlling the separation at 0.3c and $(U_j/U) = 2$. The large separation region cannot be completely removed by the jet blowing.

In the present work, the influence of aerodynamic factors on pressure coefficient in separated laminar flow around the wind turbine blades is investigated in numerical and optimization methods to improve the performance of wind turbine by observe the variation of power coefficient in deferent cases.

**Modified Strong Implicit Procedure** (M**SIP):**

Stone's method, also known as the strongly implicit procedure or SIP, is an algorithm for solving a sparse linear system of equations. The method uses an incomplete LU decomposition, which approximates the exact **LU** decomposition, to get an iterative solution of the problem. The method is named after Herbert L. Stone, who proposed it in 1968.The **LU** decomposition is an excellent general purpose linear equation solver. The biggest disadvantage is that it fails to take advantage of coefficient matrix to be a sparse matrix. The **LU** decomposition of a sparse matrix is usually not sparse, thus, for large system of equations, **LU** decomposition may require a prohibitive amount of memory and arithmetical operations. In the preconditioned iterative methods, if the preconditioner matrix **M** is a good approximation of coefficient matrix **A** then the convergence is faster[6].

A version of modified Strong Implicit Procedure method was proposed by P.L.L age in 1996[7].This article develops an algorithm to estimate the asymptotic rates of convergence of the residual vector norm of a system of equations when it is solved by the modified strong implicit procedure (MSIP). This algorithm is used to develop an adaptive optimization procedure in order to improve MSIP performance during problem solution. This eliminates the trial-and-error method usually necessary to determine the optimum value of the iteration parameter. Five problems are used to test the new algorithm. The results show that the optimized MSIP can be many times faster than the original procedure for a nonoptimal value of its iteration parameter. Algorithm of the mentioned method as follows:

For the linear system **A**x = b calculate Incomplete **LU** factorization of matrix **A**:

$Ax = (M-N)x = (LU-N)x = b$

$Mx^{(k+1)} = Nx^{(k)}+b$ , with $||M|| >> ||N||$

$Mx^{(k+1)} = LUx^{(k+1)} = c^{(k)}$

$LUx^{(k)} = L(Ux^{(k+1)}) = Ly^{(k)} = c^{(k)}$
set a guess
$k = 0$, $x^{(k)}$
$r^{(k)}=b - Ax^{(k)}$
while ( $\|r^{(k)}\|_2 \geq \varepsilon$ ) do
evaluate new right hand side
$c^{(k)} = Nx^{(k)} + b$
solve $Ly^{(k)} = c^{(k)}$ by forward substitution
$y^{(k)} = L^{-1}c^{(k)}$
solve$Ux^{(k+1)} = y^{(k)}$ by back substitution
$x^{(k+1)} = U^{-1}y^{(k)}$
end while

**Momentum theory**

The air that passes through the disc undergoes an overall change in velocity, $U_{1_} - U_w$and a rate of change of momentum equal to the overall change of velocitytimes the mass flow rate [8]:

$$\text{Rate of change of momentum} = (U_\infty - U_w)\rho A_d U_d \quad \ldots(1)$$

where; $U_d = U_\infty(1-a)$

The force causing this change of momentum comes entirely from the pressure difference across the actuator disc because the stream-tube is otherwise completely surrounded by air at atmospheric pressure, which gives zero net force. Therefore,

$$(p_d^+ - p_d^-)A_d = (U_\infty - U_w)\rho A_d U_\infty(1-a) \quad \ldots (2)$$

To obtain the pressure difference ( $p_d^+ - p_d^-$ ) Bernoulli's equation is applied separatelyto the upstream and downstream sections of the stream-tube; separate equations are necessary because the total energy is different upstream and downstream. Bernoulli's equation states that, under steady conditions, the total energy in the flow, comprising kinetic energy, static pressure energy and gravitational potentialenergy, remains constant provided no work is done on or by the fluid. Thus, for a unit volume of air [8]:

$$\frac{1}{2}\rho U^2 + p + \rho g h = const.$$

Upstream, therefore, given:

$$\frac{1}{2}\rho_\infty U_\infty^2 + \rho_\infty g h_\infty = \frac{1}{2}\rho_d U_d^2 + p_d^+ + \rho_d g h_d \quad \ldots (3)$$

Assuming the flow to be incompressible $(\rho_\infty = \rho_d)$ and horizontal $(h_\infty = h_d)$ then:

$$\frac{1}{2}\rho U_\infty^2 + p_\infty = \frac{1}{2}\rho U_d^2 + p_d^+ \quad \ldots(4)$$

Similarly, downstream:

$$\frac{1}{2}\rho U_w^2 + p_\infty = \frac{1}{2}\rho U_d^2 + p_d^- \quad \ldots(5)$$

Subtracting these equations we obtain:

$$(p_d^+ - p_d^-) = \frac{1}{2}\rho(U_\infty^2 - U_w^2)$$

Equation (2) then gives:

$$\frac{1}{2}\rho(U_\infty^2 - U_w^2)A_d = (U_\infty - U_w)\rho A_d U_\infty(1-a) \quad ...(6)$$

And so:

$$U_w = (1-2a)U_\infty \quad ...(7)$$

That is, half the axial speed loss in the stream.

**Power coefficient**

The force on the air becomes, from Equation (2) [8]:

$$F = \left(p_d^+ - p_d^-\right)A_d = 2\rho A_d U_\infty^2\, a(1-a) \quad ...(8)$$

As this force is concentrated at the actuator disc the rate of work done by the force is$FU_d$ and hence the power extraction from the air is given by**:**

$$Power = FU_d = 2\rho A_d U_\infty^3\, a(1-a)^2 \quad ...(9)$$

A power coefficient is then defined as**:**

$$C_p = \frac{power}{\frac{1}{2}\rho A_d U_\infty^3} \quad ...(10)$$

where the denominator represents the power available in the air, in the absence of the actuator disc. Therefore:

$$C_p = 4\,a(1-a)^2 \quad ...(11)$$

**The Betz limit**

The maximum value of $C_p$ occurs when [8]:

$$\frac{dC_p}{da} = 4(1-a)(1-3a) = 0$$

which gives a value of $a = \frac{1}{3}$

Hence; $C_{p_{max}} = \frac{16}{27} = 0.593$ ...(12)

The maximum achievable value of the power coefficient is known as the Betz limit after Albert Betz [9] and, to date, no wind turbine has been designed which is capable of exceeding this limit. The limit is caused not by any deficiency in design, for, as yet, we have no design, but because the stream-tube has to expand upstream of the actuator disc and so the cross section of the tube where the air is at the full, free-stream velocity is smaller than the area of the disc. $C_p$could, perhaps, more fairly be defined as:

$$C_p = \frac{Power\ extracted}{Power\ available} = \frac{Power\ extracted}{\frac{16}{27}\left(\frac{1}{2}\rho U_\infty^3 A_d\right)}$$

**Determination of rotor power coefficient and turque:**

The tangential velocity will not be the same for all radial positions and it may well also be that the axial induced velocity is not the same. To allow for variation of both induced velocity components consider only an annular ring of the rotor disc which is of radius $r$ and of radial width$\delta r$.The increment of rotor torque acting on the annular ring will be responsible forimparting the tangential velocity component to the air whereas the axial force acting on the ring will be responsible for the reduction in axial velocity. The whole disc comprises a multiplicity of annular rings and each ring

is assumed to act independently in imparting momentum only to the air which actually passes through the ring.

The torque on the ring will be equal to the rate of change of angular momentumof the air passing through the ring. Thus,

torque = rate of change of angular momentum

= mass flow rate × change of tangential velocity × radius

$$\delta Q = \rho \delta A_d U_\infty (1-a) 2\Omega a' r^2 \quad \ldots(13)$$

where$\delta A_d$ is taken as being the area of an annular ring.The driving torque on the rotor shaft is also $\delta Q$ and so the increment of rotorshaft power output is:

$$\delta P = \delta Q \Omega$$

The total power extracted from the wind by slowing it down is therefore determinedby the rate of change of axial momentum given by eq.(9).

$$\delta P = 2\rho \delta A_d U_\infty^3 a(1-a)^2$$

Hence;

$$2\rho \delta A_d U_\infty^3 a(1-a)^2 = \rho \delta A_d U_\infty (1-a) 2\Omega a' r^2$$

And;

$$U_\infty^2 a(1-a) = \Omega^2 a' r^2$$

$\Omega r$is the tangential velocity of the spinning annular ring and so $\lambda = \Omega r / U_\infty$ iscalled the local speed ratio. At the edge of the disc $r = R$ and $\lambda = \Omega r / U_\infty$ is knownat the tip speed ratio. Thus

$$a(1-a) = \lambda_r^2 a' \quad \ldots(14)$$

The area of the ring is $\delta A_d = 2\pi r \delta r$, therefore the incremental shaft power is, from equation (13):

$$\delta P = dQ\Omega = \left(\frac{1}{2}\rho U_\infty^3 2\pi r \delta r\right) 4a'(1-a)\lambda_r^2$$

The term in brackets represents the power flux through the annulus, the termoutside the brackets, therefore, is the efficiency of the blade element in capturingthe power, or blade element efficiency:

$$\eta_r = 4a'(1-a)\lambda_r^2$$

In terms of power coefficient:

$$\frac{d}{dr}C_p = \frac{4\rho U_\infty^3 \pi r a'(1-a)\lambda_r^2}{\frac{1}{2}\rho U_\infty^3 \pi R} = \frac{8a'(1-a)\lambda_r^2 r}{R^2}$$

$$\frac{d}{d\mu}C_p = 8a'(1-a)\lambda_r^2 \mu^3 \quad \ldots(15)$$

where $\mu = r/R$.

Knowing how $a$ and $a'$ vary radially, equation (15) can be integrated to determine the overall power coefficient for the disc for a given tip speed ratio, $\lambda$.

**RESULTS AND DISCUSSIONS:**

**The Computer Program**: The program solves for the dependent variables in an iterative manner. Within each iteration, the individual variables U, V, P, k and ε are solved. During the calculation, the field residuals are monitored. The iteration scheme is continued until the results converge, i.e. until the normalized field residuals have fallen below a prescribed upper limit as low as $10^{-9}$ when laminar flows are predicted

and they dropped to as low as $(10^{-5} - 10^{-8})$ in the case of turbulent flows[10].The program is very well structured and highly organized for a wide range of different problems (belonging to the present work field of engineering application). The developed numerical method is fully second order accurate, and in combination with the SIP solver, based on SIMPLE-algorithm.

**Securing Convergence:** Because the solution procedures are essentially iterative, it is inevitable that some adjustments shall be carried out before the solution has converged sufficiently for the computation to be terminated. Divergence is caused by the tendency of the residuals in one or more equations to increase rather than decrease as the iterations proceed and it is usually accompanied by the appearance of unphysically large values in some of the dependent variables. It should be mentioned here that divergence usually occurs due to the error in the input data. When divergence occurs, it is necessary to establish the cause ; this is usually to be found in the strength of the linkages between two or more sets of equations. For example if a problem of convection heat transfer is being solved, the two-way interaction between the temperature field and the velocity field, whereby each influences the other, is a possible source of divergence. Whether it is the source in a particular case is easily established by freezing the temperature field before the divergence has progressed too far, and then observing if the divergence continues. If it does not, the velocity-temperature link can be regarded as the source of divergence; otherwise, the cause must be searched in some other linkages.

To apply freezing, the simplest way is to under-relax heavily. In this way, one can investigate the contributions to divergence of linkages between individual velocity components or between turbulence energy and its dissipation rate in a turbulent flow. If freezing by very severe under-relaxation restores convergent behavior it is obviously possible that modest under-relaxation will have the same qualitative tendency, which allows the solution to proceed so that all residuals do finally diminish. The use of under-relaxation factor is a common means of securing convergence in practice. If under-relaxation factor is employed indiscriminately, it can lead to waste of computer time. However, when it is applied to only those equations that have been identified as potential cause of divergence, and with the amount that is necessary to procure convergence, it is a good second-recourse remedy to apply. The first-recourse is to check the in-data.

**Grid Independence Solution:** One way to establish accurate results is to obtain simulations that are grid independent. This means that the results will be relatively constant even if the simulations would be performed on a mesh with smaller computational cells. Smaller cell sizes lead to more accurate results but also to an increased number of cells in the domain, which will increase the CPU time per iteration. The perfect mesh is thus a domain where the size of the cells is as large as possible without any significant change in the results.

Grid independence tests can be carried out in order to obtain this perfect mesh. The idea is to perform a number of simulations with identical starting conditions on a specific geometry using different cell sizes for the mesh. If no significant deviation in the results is found between the simulations, grid independence is achieved.

Airfoil domain and their computation grid are the most sensitive computation areas; hence, the number of the grid points in this domain is most critical. To test for

grid independence, five sets of grids, with increasing grid density are studied. The different grids are employed to compute the airfoil flow with the same conditions. They have (72×24) for the first grid, (152×36) for the second and (208×40) for the third and (248*44) for fourth and (280*47) for the fifth one. The finest grid has 28033, 88305, 134113, 181866 and 219333 cells, whereas the coarsest has 1752, 5661, 8569, 11249 and 13567 cells. The middle one has 7105, 22265, 33777, 45466 and 54833 cells. The differences in the computational results between set 1 and set 2, and between set 2 and set 3, are less than 3% and the results between set 3 and sets 4,5 are 0.1% . Because the results from the third and fourth and fifth gird less differ from each other, it can be concluded that the third gird has enough spatial resolution to the flow.

**Flow Field Distributions:** Figures (1) to(15) show the airflow around a NACA 4415 airfoil from a 0° angle of attack to a 15° angle of attack at $U = 5.0$. At the 5° angle of attack, the airflow is described as streamline and there is no appreciable turbulence or circulation. At angles of attack 5° and 10° , the streamlines above the leading edge begin to crowd together more than they did at a lower angle of attack. This causes an increase of velocity above the upper surface and consequently a reduction of pressure; hence, lift is increasing. At each successive increase of the angle of attack, the point at which the airflow breaks away from the upper surfaces moves forward, and this increases the amount of burbling or turbulence (burble is a breakdown of streamline airflow about a body), seen that where burbling occurs on a surface, the pressure cannot drop below atmospheric and the failure to have a region of pressure differential destroys lift in that region. At a very high angle of attack, burbling is so excessive that the drag may be even greater than the lift. The separation or circulation is very clear at $\alpha = 15°$.

**Blowing Effect on the airfoil:** At low Reynolds number and the angle of attack of the flow exceeds a certain critical angle, the flow does not reach the trailing edge, but leaves the surface at the separation position. Beyond this position the flow direction is reversed. A blowing technique exceeds the less energy from the flow when it is separated. This is used to control the airfoil separation. In this work for controlling the separation, air blowing (not suction) is used because the effect of blowing is larger and perfect in the leading edge [11].

From Figure (16) to (18) at NACA 4415 and U=5.0 , for $\alpha = 5^o$ ،$10^o$ ،$15^o$, and the ratio between power coefficient and tip speed ratio for with and without air blowing. It seen that for chord equal to one and alpha equal to five, the power coefficient is greater than the $\alpha = 10^o$ ،$15^o$ at two cases with and without air blowing. For $\alpha = 5^o$ ،$10^o$ ،$15^o$the power coefficient with air blowing is greater than the without blowing, and for two cases (with and without air blowing), for $\alpha = 5^o$ ، $10^o$ ،$15^o$and tip speed ratio=2.5 is greater than the other.

**REFERENCES:**

[1] Bobonea A.," Impact Of Pulsed Blowing Jet On Aerodynamic Characteristics Of Wind Turbine Airfoils", 9th International Conference On Mathematical Problems In Engineering, Aerospace And Sciences, Volume 1493, Pp. 170-174, 2012.

[2]Bokserv.D., Petrova. V. And Savinp. V.," Experimental Study Of Tangential Blowing Effect Of Supersonic Jet On Aerodynamics Of A Supercritical Wing At Transonic Speeds",Tsagi Science Journal , Volume 42, P.P 427-444, 2011.
[3]Campbell, G. A., Obot, N. T. And Cao, B.," Aerodynamics In The Blown Film Process", Polymengsci, Vol.32, P.P751–759, Doi: 10.1002/Pen.760321107,2004.
[4]Jiang, P., Wang, Z. J. And Gursul, I., "Effects Of Unsteady Trailing-Edge Blowing On Delta Wing Aerodynamics". *Journal Of Aircraft*, 47 (2), Pp. 591-602, 2010.
[5]Yasser A.M.,"Control Of Separation For Naca 2412 Airfoil At Different Angle Of Attack Using Air Blowing" Ph. D. Thesis Presented To The University Of Technology, 2009.
[6]Acosta, J.M., " Numerical Algorithms For Two Dimensional Computational Fluid Dynamic Problems. Phd Thesis.Polytechnic University Of Catalunia, 2001.
[7]Lagep.L.' "Modified Strong Implicit Procedure With Adaptive Optimization Of Its Iteration Parameter", Journal Citation Reportsvolume 30, Issue 3, P.P255-270, 2007.
[8]Burton T., Sharpe D., N. Jenkins, Bossanyie., "Wind Energy Handbook", John Wiley & Sons, Ltd, 2001.
[9]Eggleston, D. M. And Stoddard, F. S., " Wind Turbine Engineering Design", Van Nostrand Reinhold Company, New York, (1987).
[10]Peric, M., "A Finite Volume Method For The Prediction Of Three-Dimensional Fluid Flow In Complex Ducts", Ph.D. Thesis, Imperial College, 1985.
[11] Huang, P.G. "Single Suction/Blowing Jet Study" Chapter (4), University Of Kentucky, 1979.

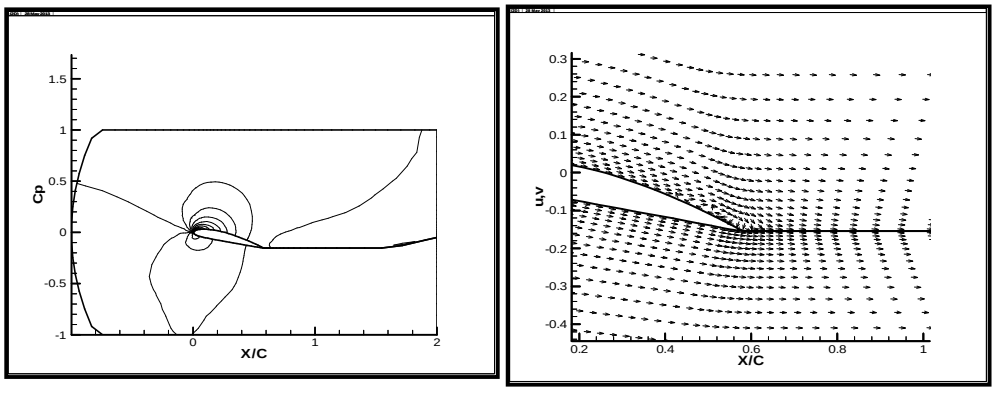


**(a)**

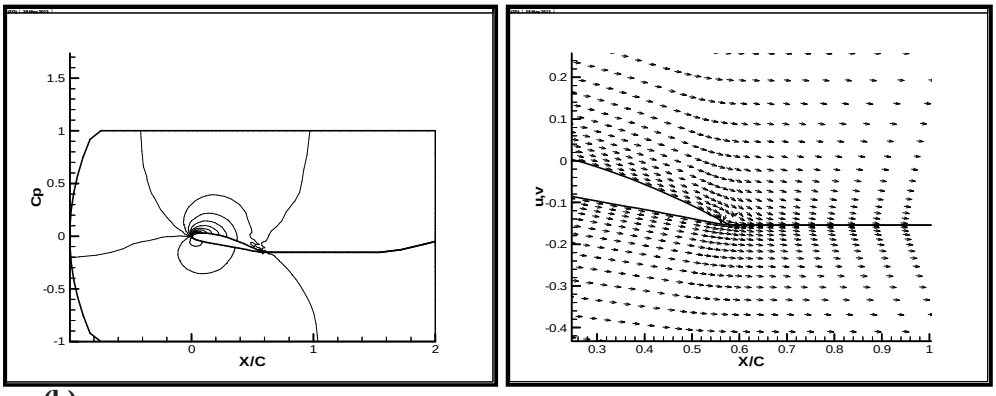


**(b)**

**Figure (1)Pressure distribution and flow stream of NACA 4415 at $chord = 0.6, \alpha = 10^o, U = 5.0$**

**(a) without blowing. (b)with blowing (at $\alpha_{blowing} = -10^o$ and $U_{blowing} = 10$)**

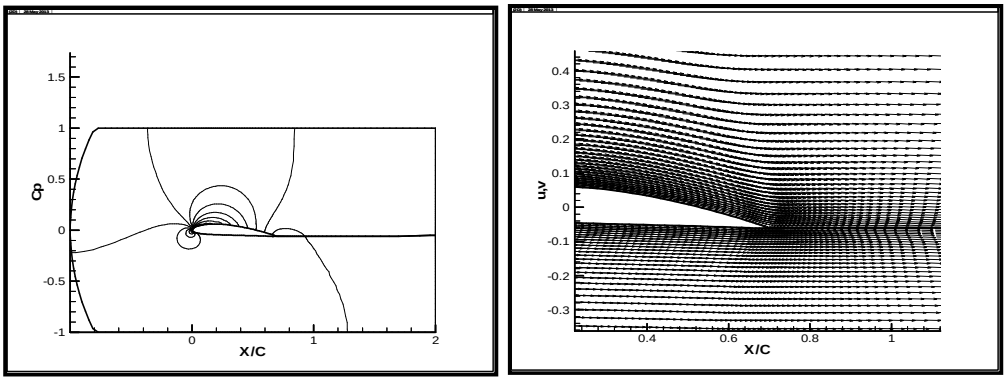


**(a)**

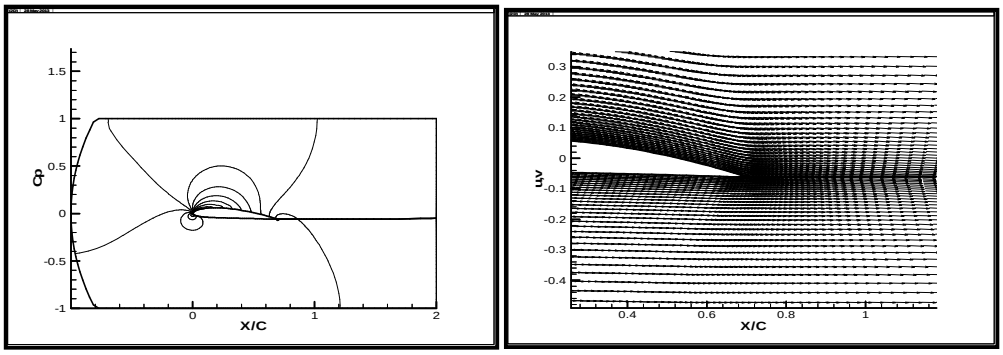


**(b)**

**Figure (2)Pressure distribution and flow stream of NACA 4415 at $chord = 0.6, \alpha = 10^o, U = 5.0$**

**(a) without blowing. (b)with blowing (at $\alpha_{blowing} = -10^o$ and $U_{blowing} = 10$)**

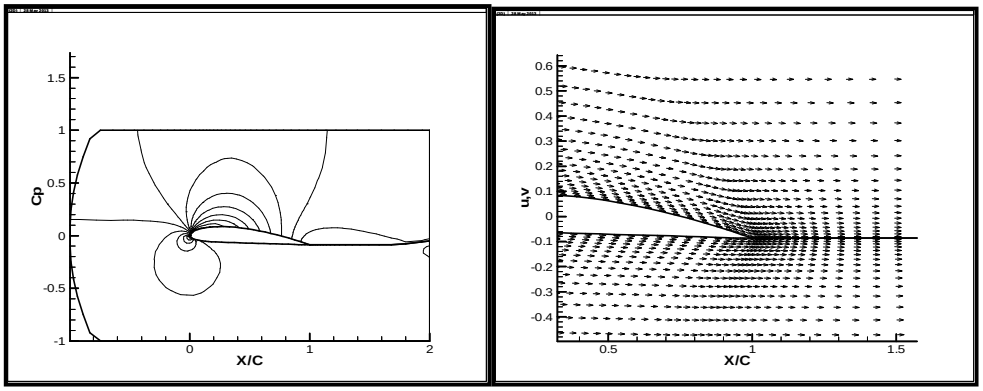


**(a)**

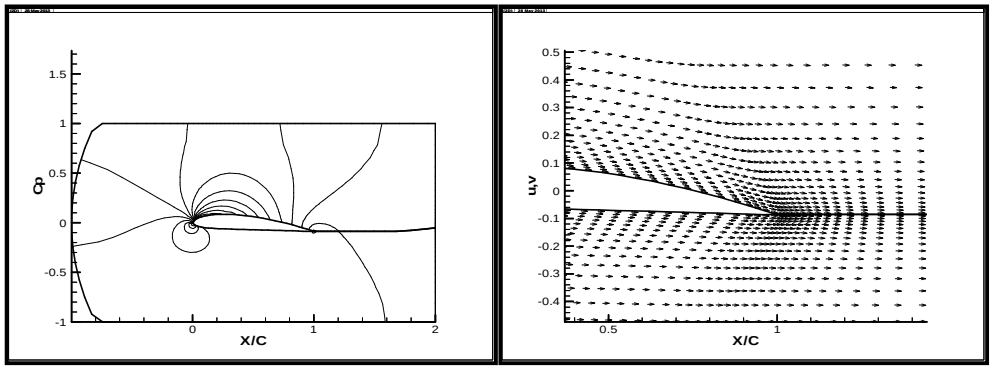


**(b)**

**Figure (3)Pressure distribution and flow stream of NACA 4415 at $chord = 0.6, \alpha = 15^o, U = 5.0$**
**(a) without blowing. (b)with blowing (at $\alpha_{blowing} = -10^o$ and $U_{blowing} = 10$)**

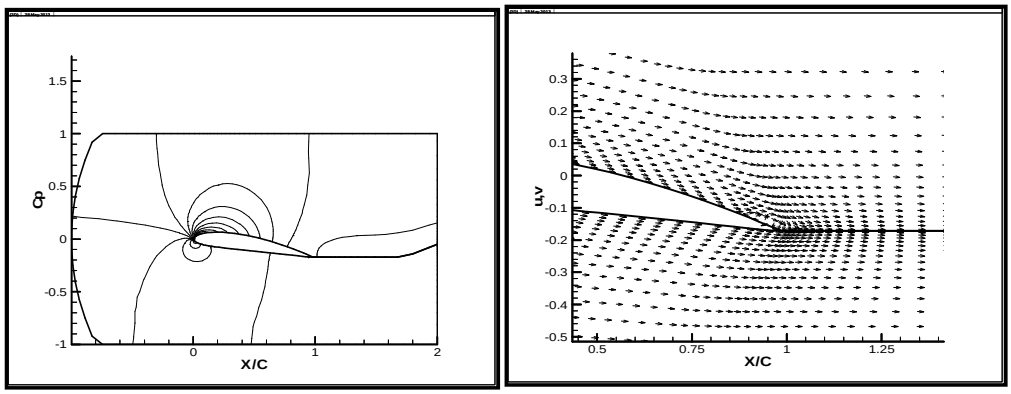


**(a)**

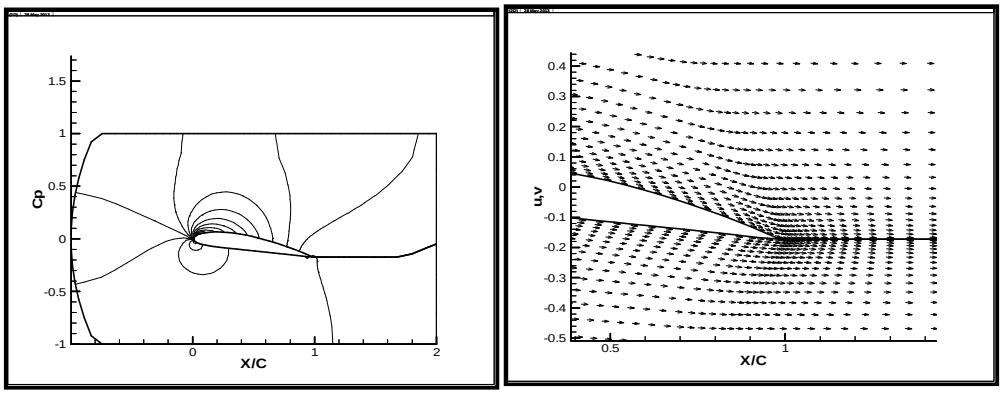


**(b)**

**Figure (4)Pressure distribution and flow stream of NACA 4415 at $chord = 0.7, \alpha = 5^o, U = 5.0$**
**(a) without blowing. (b)with blowing (at $\alpha_{blowing} = -10^o$ and $U_{blowing} = 10$)**

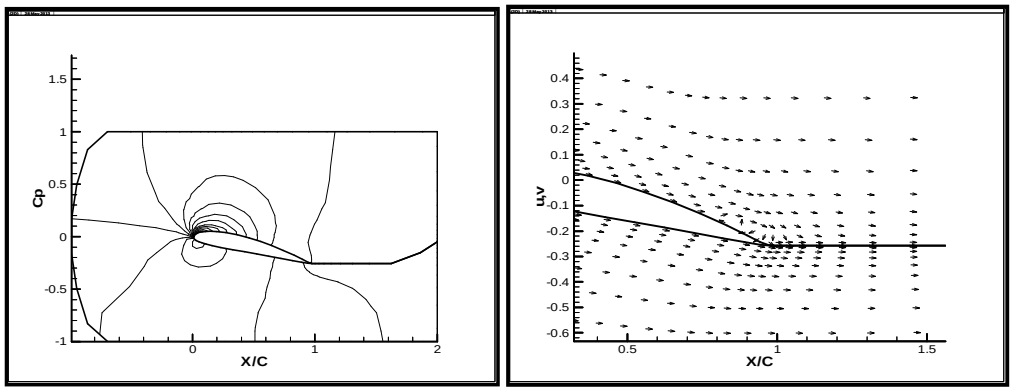


**(a)**

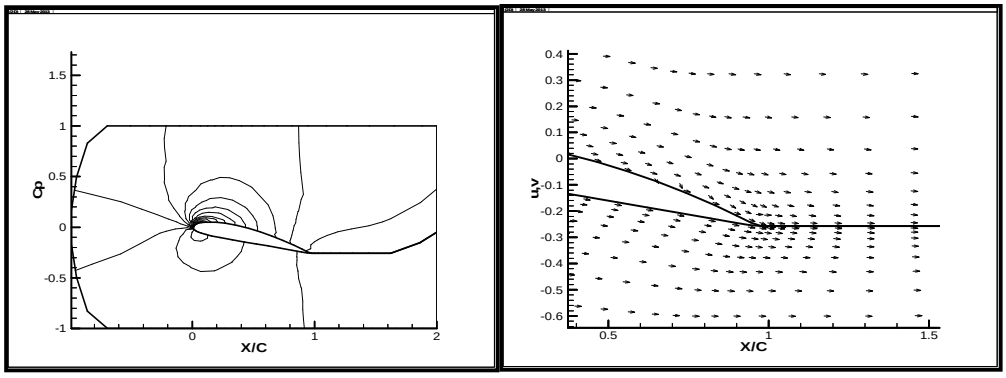


**(b)**

**Figure (5)Pressure distribution and flow stream of NACA 4415 at $chord = 0.7, \alpha = 10^o, U = 5.0$**
**(a) without blowing. (b)with blowing (at $\alpha_{blowing} = -10^o$ and $U_{blowing} = 10$)**

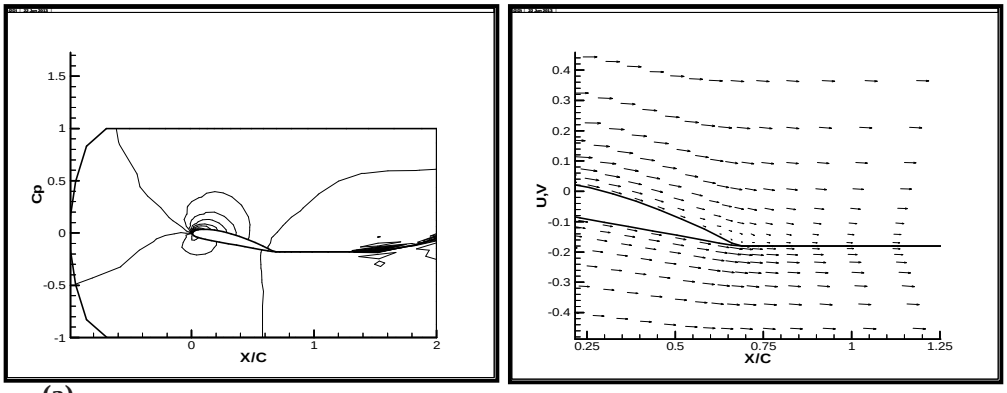


**(a)**

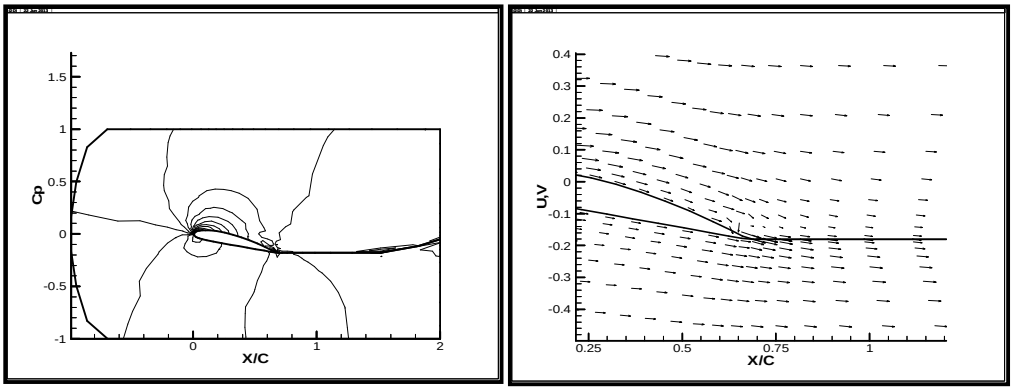


**(b)**

**Figure (6)Pressure distribution and flow stream of NACA 4415 at $chord = 0.7, \alpha = 15^o, U = 5.0$**
**(a) without blowing. (b)with blowing (at $\alpha_{blowing} = -10^o$ and $U_{blowing} = 10$)**

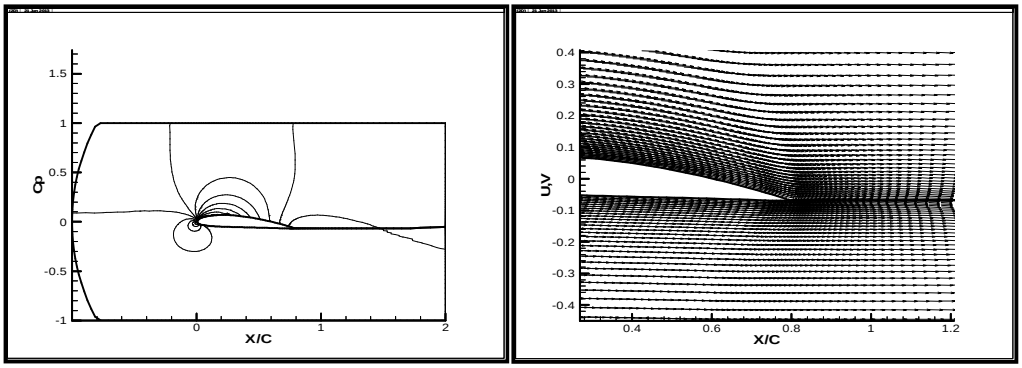


**(a)**

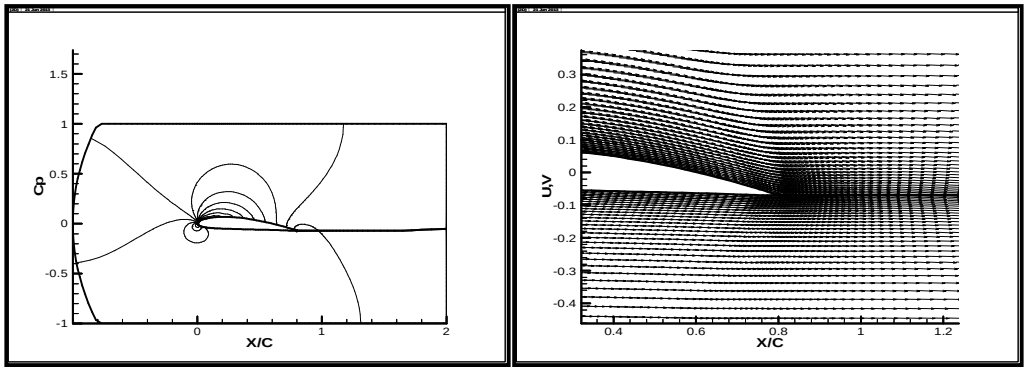


**(b)**

**Figure (7)Pressure distribution and flow stream of NACA 4415 at $chord = 0.8, \alpha = 5^o, U = 5.0$**
**(a) without blowing. (b)with blowing (at $\alpha_{blowing} = -10^o$ and $U_{blowing} = 10$)**

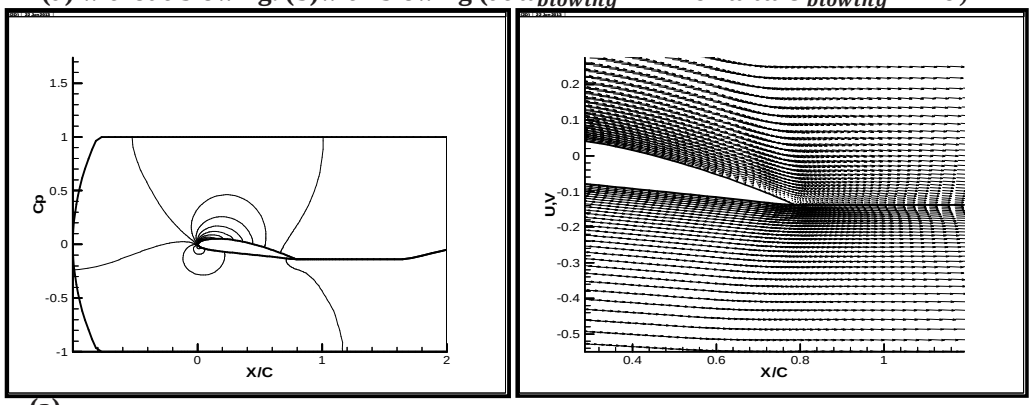


**(a)**

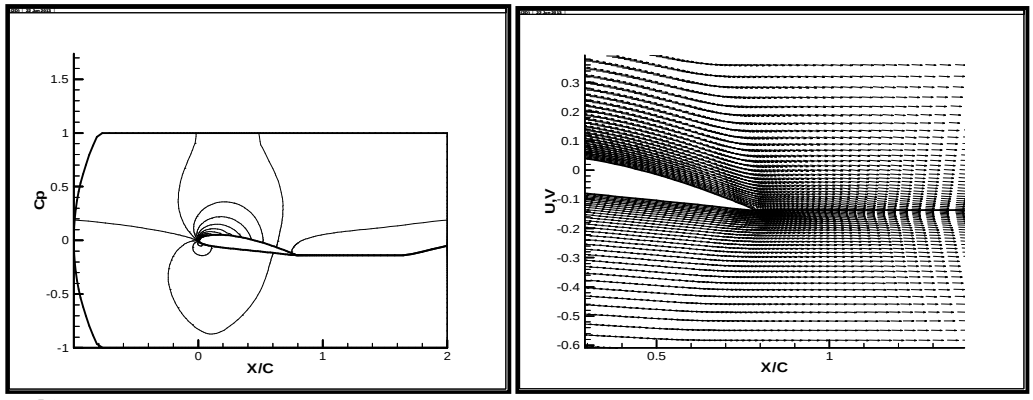


**(b)**

**Figure (8)Pressure distribution and flow stream of NACA 4415 at $chord = 0.8, \alpha = 10^o, U = 5.0$**
**(a) without blowing. (b)with blowing (at $\alpha_{blowing} = -10^o$ and $U_{blowing} = 10$)**

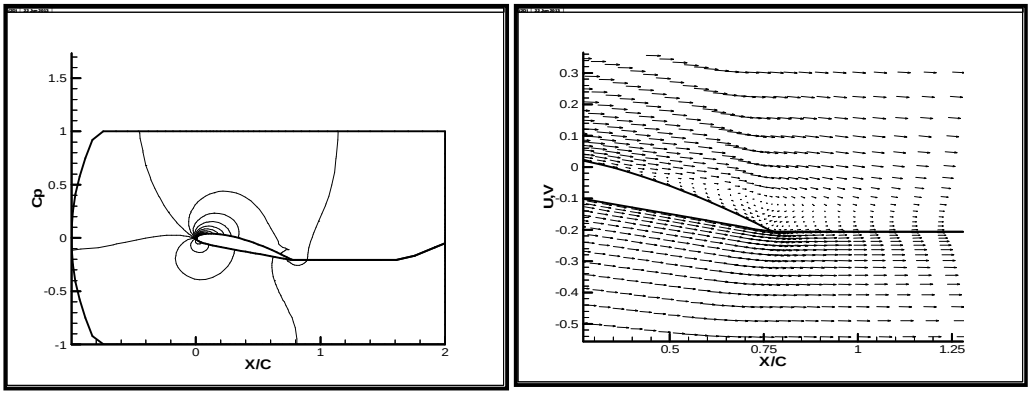


**(a)**

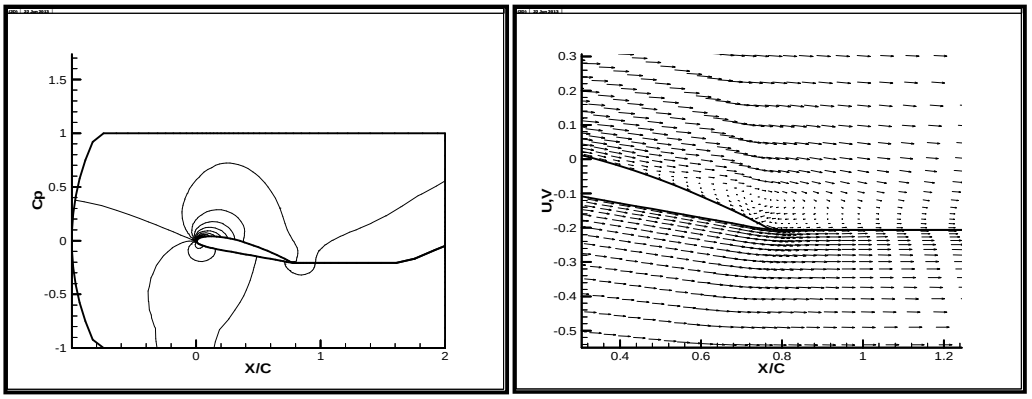


**(b)**

**Figure (9)Pressure distribution and flow stream of NACA 4415 at $chord = 0.8, \alpha = 15^o, U = 5.0$**
**(a) without blowing. (b)with blowing (at $\alpha_{blowing} = -10^o$ and $U_{blowing} = 10$)**

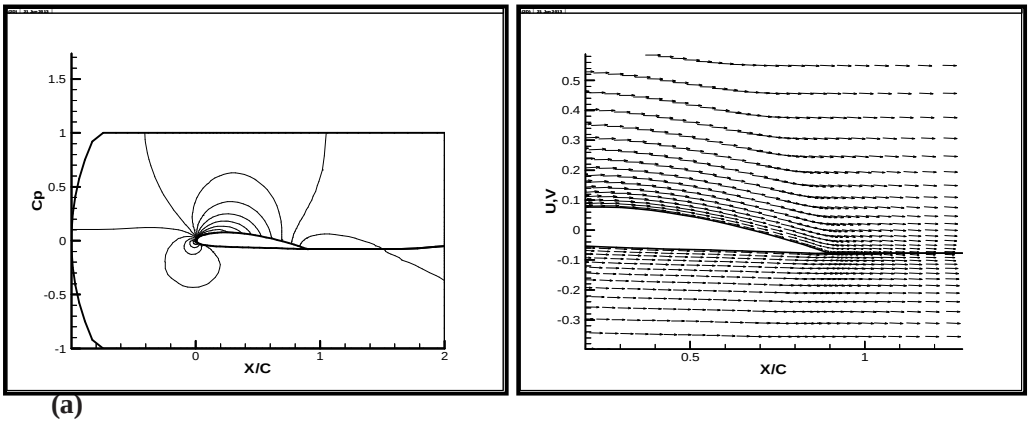


**(a)**

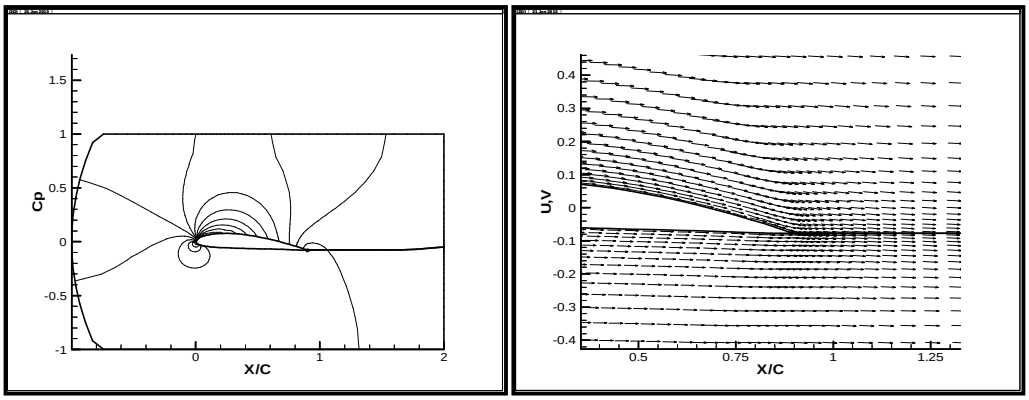


**(b)**

**Figure (10)Pressure distribution and flow stream of NACA 4415 at $chord = 0.9, \alpha = 5^o, U = 5.0$**

**(a) without blowing. (b)with blowing (at $\alpha_{blowing} = -10^o$ and $U_{blowing} = 10$)**

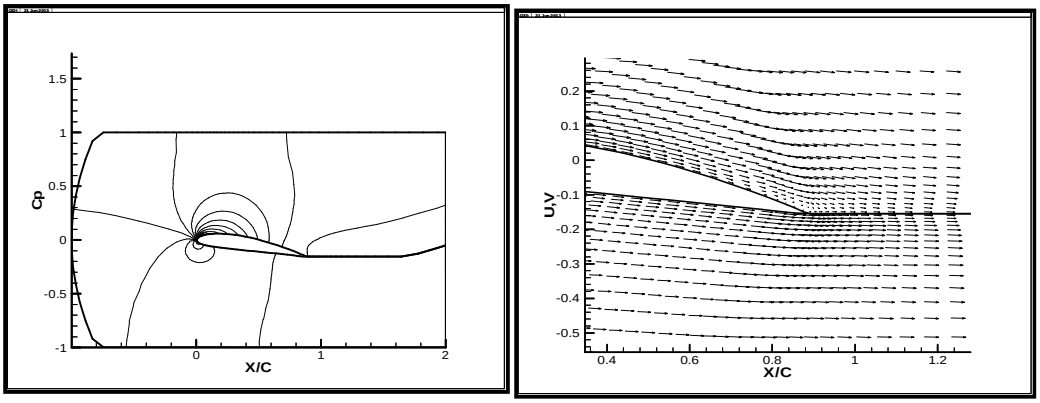


(a)

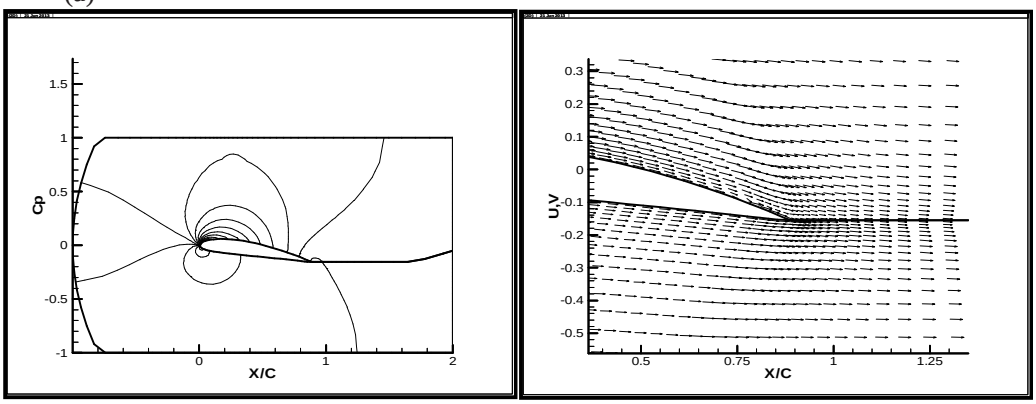


**Figure (11)Pressure distribution and flow stream of NACA 4415 at $chord = 0.9, \alpha = 10^o, U = 5.0$**

**(a) without blowing. (b)with blowing (at $\alpha_{blowing} = -10^o$ and $U_{blowing} = 10$)**

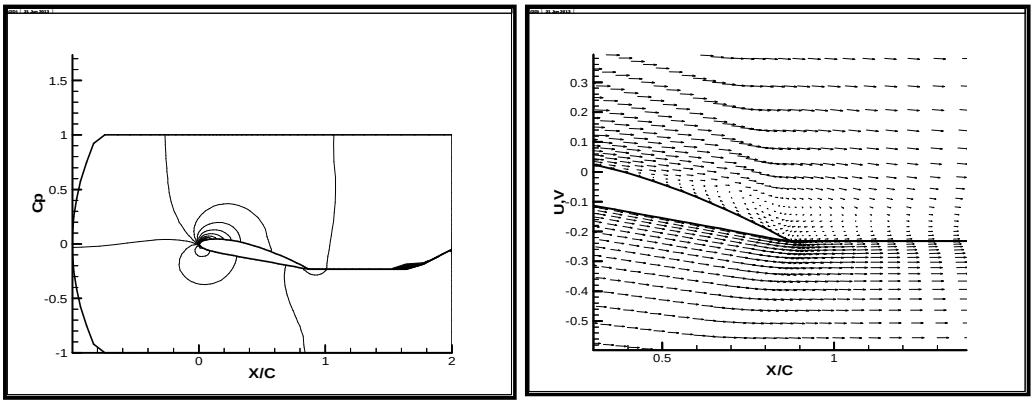


(a)

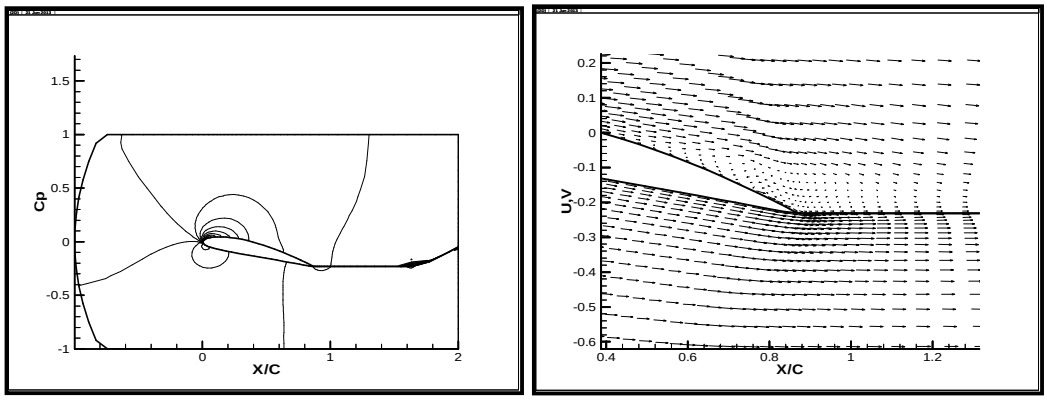


(b)

**Figure (12)Pressure distribution and flow stream of NACA 4415 at $chord = 0.9, \alpha = 15^o, U = 5.0$**
**(a) without blowing. (b)with blowing (at $\alpha_{blowing} = -10^o$ and $U_{blowing} = 10$)**

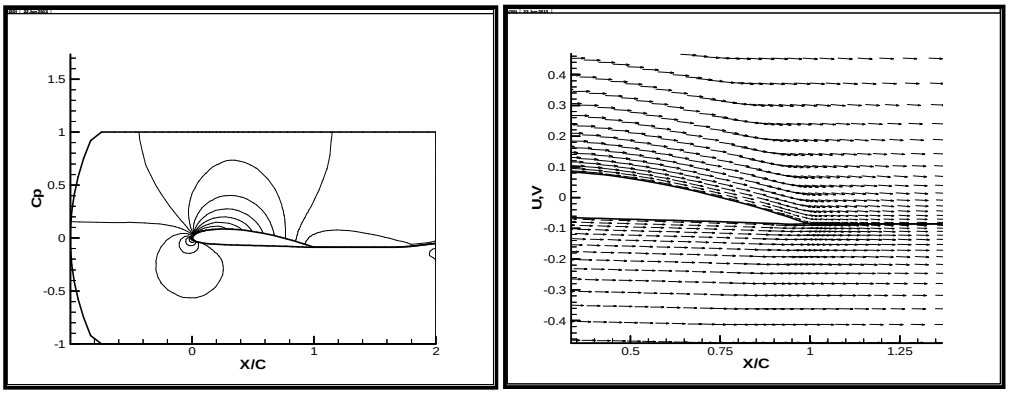


**(a)**

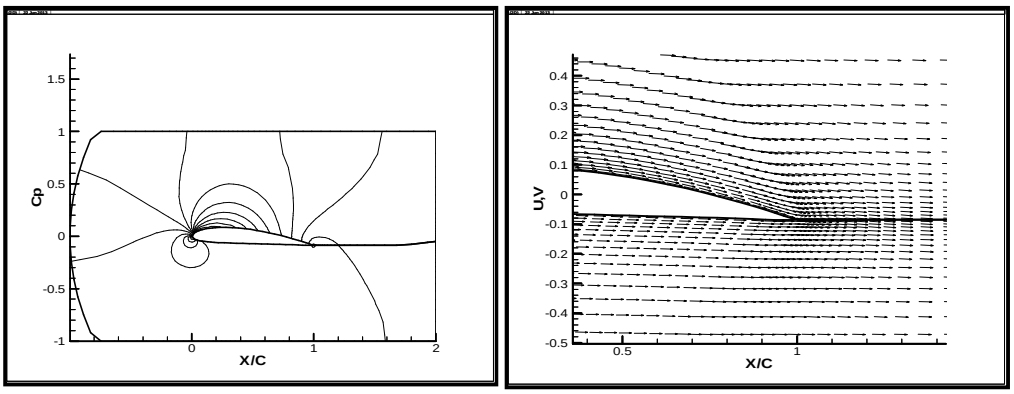


**(b)**

**Figure (13)Pressure distribution and flow stream of NACA 4415 at $chord = 1.0, \alpha = 5^o, U = 5.0$**

**(a) without blowing. (b)with blowing (at $\alpha_{blowing} = -10^o$ and $U_{blowing} = 10$)**

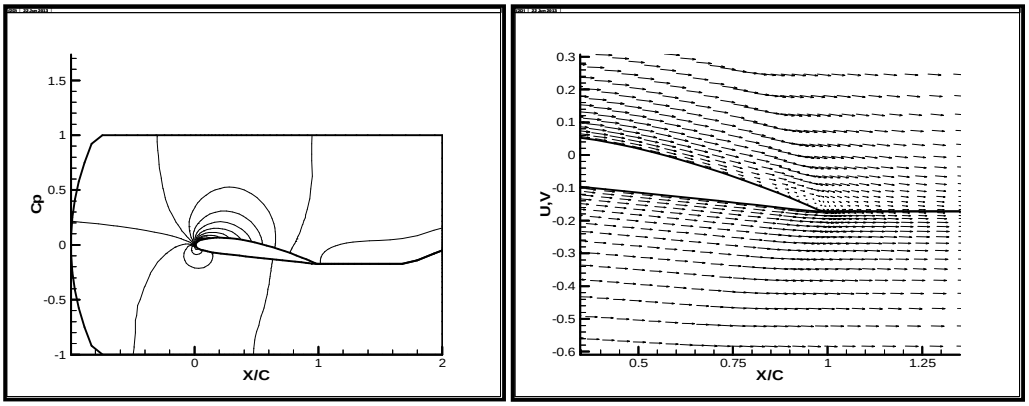


**(a)**

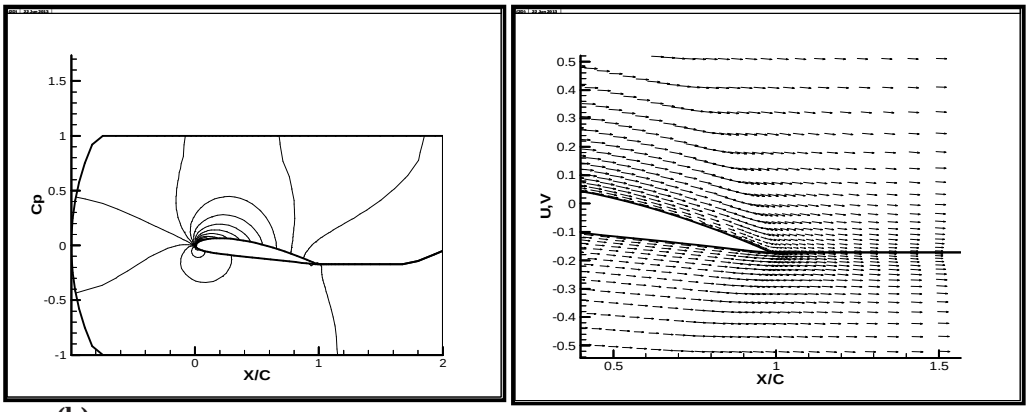


**(b)**

**Figure (14)Pressure distribution and flow stream of NACA 4415 at $chord = 1.0, \alpha = 10^o, U = 5.0$**

**(a) without blowing. (b)with blowing (at $\alpha_{blowing} = -10^o$ and $U_{blowing} = 10$)**

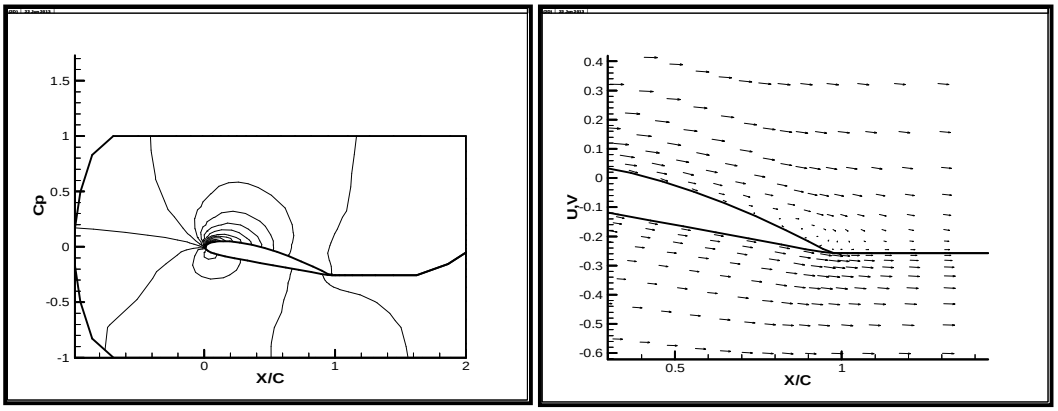


**(a)**

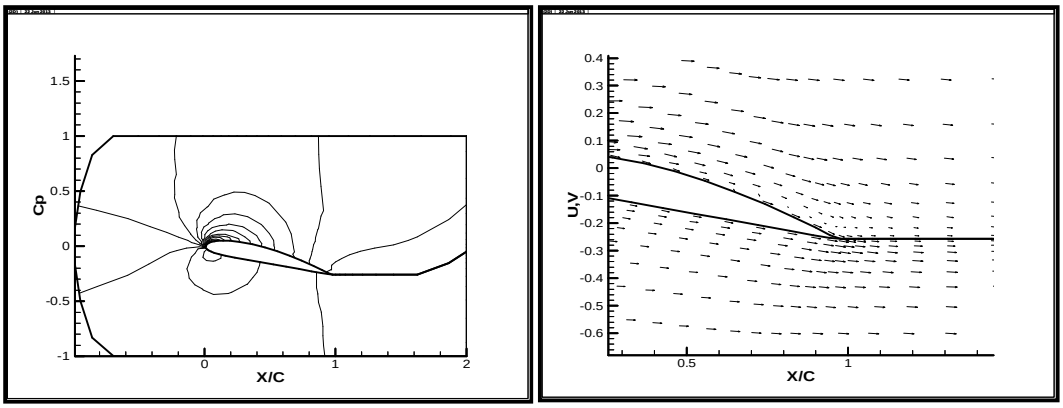


**(b)**

**Figure (15)Pressure distribution and flow stream of NACA 4415 at $chord = 1.0, \alpha = 15^o, U = 5.0$**
**(a) without blowing. (b)with blowing (at $\alpha_{blowing} = -10^o$ and $U_{blowing} = 10$)**

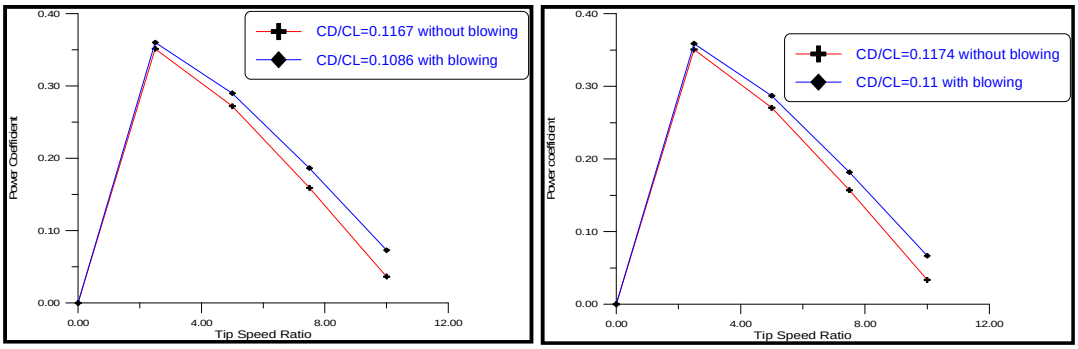


(a) NACA 4415 at chord 1.0 (b) NACA 4415 at chord 0.9

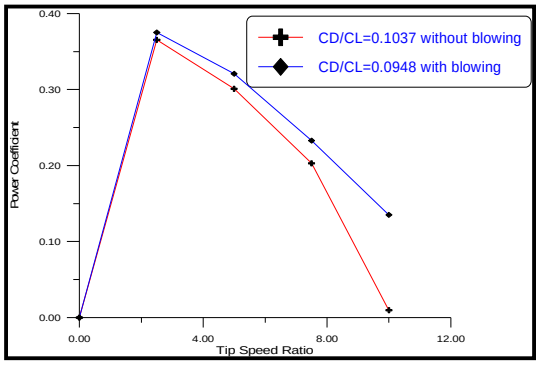


(c) NACA 4415 at chord 0.8

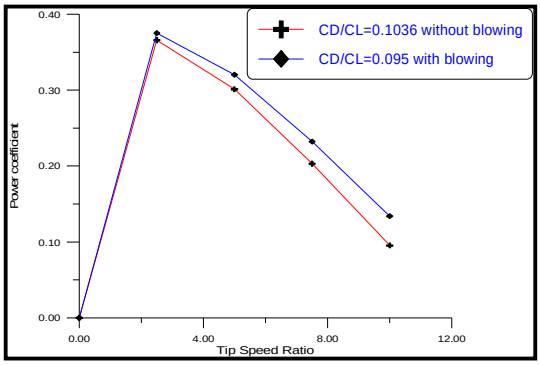


(d) NACA 4415 at chord 0.7

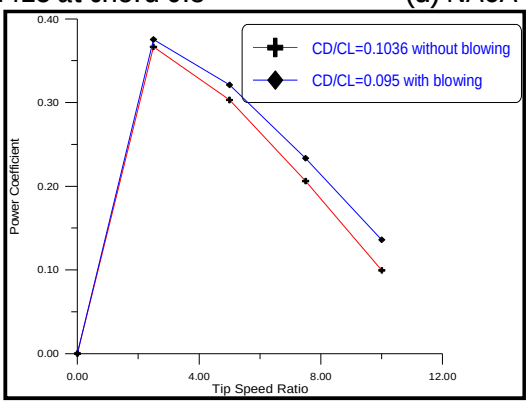


(e) NACA 4415 at chord 0.6

**Figure (16)The relation between power coefficient and tip speed ratio at $\alpha = 5^o$ and $U = 5.0$ for different $C_D/C_l$ ratio**

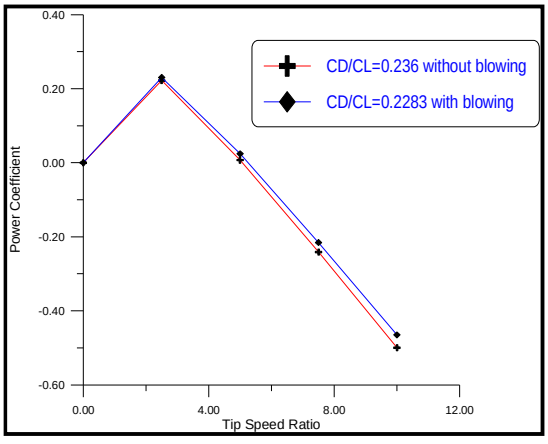


(a) NACA 4415 at chord 1.0

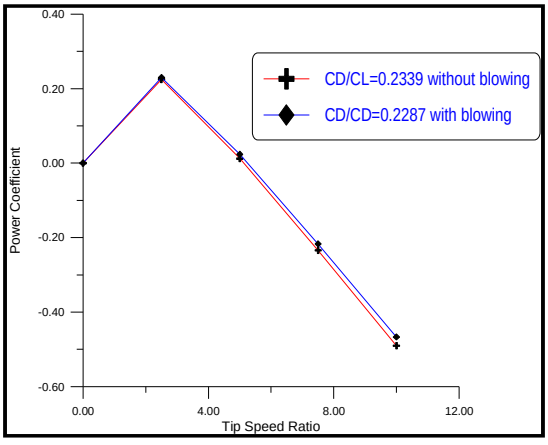


(b) NACA 4415 at chord 0.9

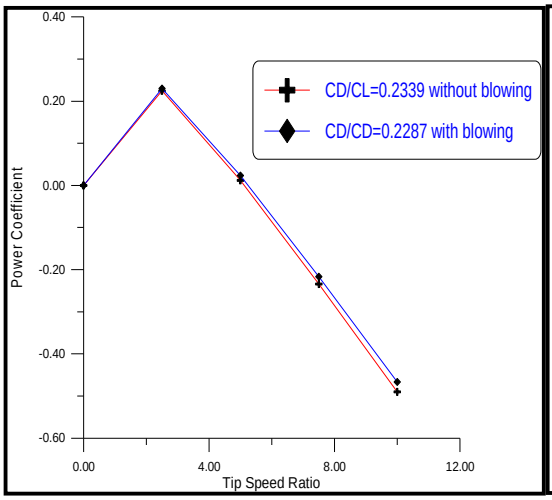


(c) NACA 4415 at chord 0.8

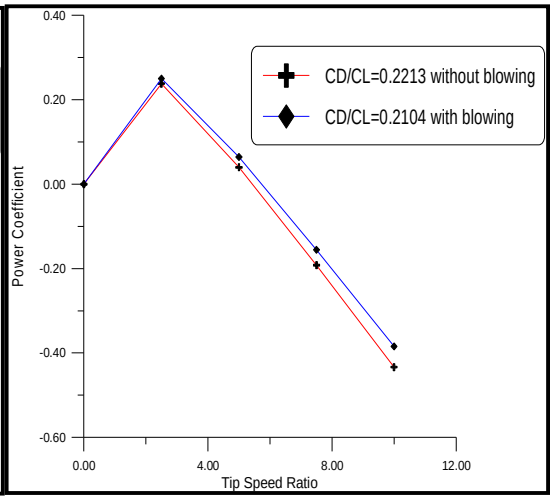


(d) NACA 4415 at chord 0.7

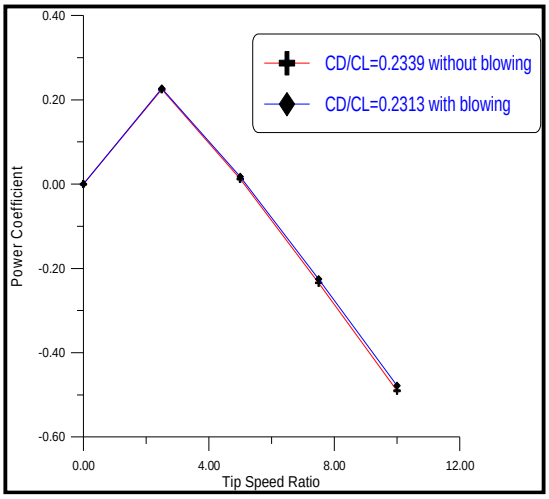


(e) NACA 4415 at chord 0.6

**Figure (17)The relation between power coefficient and tip speed ratio at $\alpha = 10^o$ and $U = 5.0$ for different $C_D/C_l$ ratio**

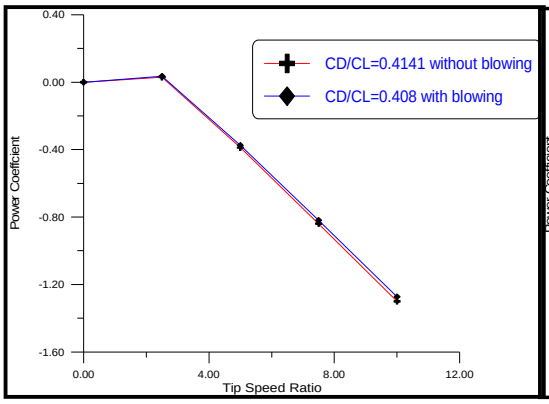


(a) NACA 4415 at chord 1.0

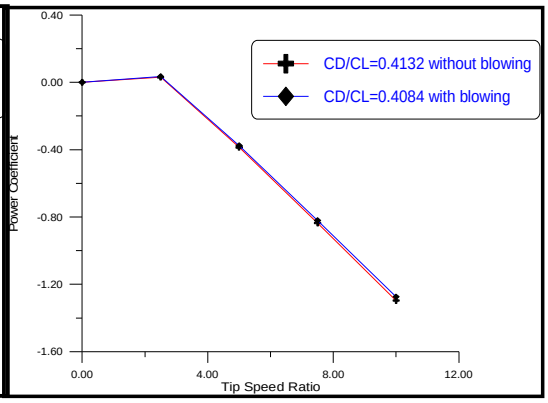


(b) NACA 4415 at chord 0.9

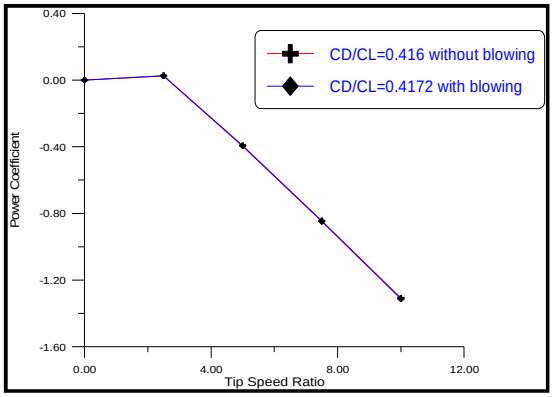


(c) NACA 4415 at chord 0.8

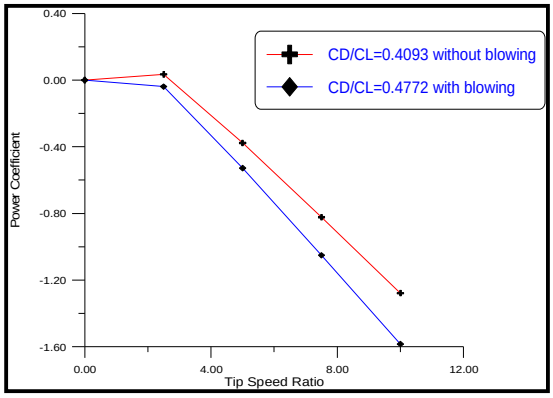


(d) NACA 4415 at chord 0.7

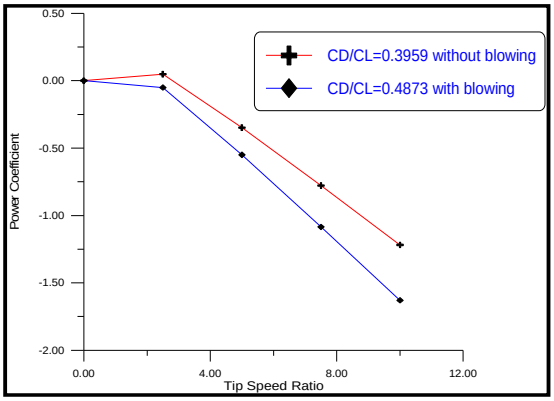


(e) NACA 4415 at chord 0.6

**Figure (18)The relation between power coefficient and tip speed ratio at $\alpha = 15^{o}$ and $U = 5.0$ for different $C_D/C_l$ ratio.**